CORROSION SCIENCE AND TECHNOLOGY, Vol.25, No.2(2026), pp.88~103 pISSN 1598-6462 / eISSN 2288-6524
[Research Paper] DOI: https://doi.org/10.14773/cst.2026.25.2.88

Characteristics of Corrosion Resistance and Microstructural Analysis of AlSi and Zn Coated Hot Press Forming Steels

Hye-Jin Kim†, Ei-Joon Shim, Ho-Jun Choi, and Yoori Kim

Department of Advanced Materials Engineering, Tech University of Korea (TU Korea), Siheung-si, Gyeonggi-do, 15073, Republic of Korea

(Received April 07, 2026; Revised April 22, 2026; Accepted April 22, 2026)

Hot press forming (HPF) steels are widely used in automotive applications; however, their corrosion performance is significantly influenced by the coating microstructure. Although Al–Si and Zn-based coatings are commonly applied, the relationship between microstructural characteristics and electrochemical behavior is not yet well understood. This study investigates the corrosion behavior of Al–Si-coated and Zn-coated HPF steels using an integrated approach that combines electron backscatter diffraction (EBSD) analysis with electrochemical techniques. Microstructural characteristics were directly correlated with electrochemical responses obtained from open circuit potential (OCP), electrochemical impedance spectroscopy (EIS), potentiodynamic polarization, and galvanostatic testing. The Al–Si-coated HPF exhibited a dense and continuous Fe–Al intermetallic multilayer structure, which provides effective barrier-type protection and stable electrochemical behavior. In contrast, the Zn-coated HPF displayed a heterogeneous microstructure with Fe–Zn phases and surface oxides, leading to localized electrochemical activity. EIS results indicated a simple and stable response for the Al–Si coating, while the Zn coating exhibited complex behavior associated with adsorption-related processes. These findings were consistent with polarization and galvanostatic results, confirming higher corrosion activity in the Zn coating. Overall, this study demonstrates that the corrosion behavior is strongly governed by coating microstructure, highlighting its importance in understanding corrosion mechanisms.

Keywords: *Hot press formed steel, Al-Si coating, Zn coating, Microstructure, Electrochemical technique*

1. Introduction

Hot press forming (HPF) technology has become a key manufacturing process for producing ultra-high-strength steel components in the automotive industry, particularly for safety-critical structural applications [1,2]. The use of boron steels such as 22MnB5 enables the formation of fully martensitic microstructures through rapid die quenching after austenitization, resulting in tensile strengths exceeding 1500 MPa. This high strength-to-weight ratio significantly contributes to vehicle lightweighting and improved crash performance, making HPF steels essential for next-generation automotive design. Despite these advantages, the HPF process involves heating the steel to temperatures above 900 °C, which inevitably leads to severe surface oxidation and decarburization [3]. These high-temperature-induced phenomena degrade surface integrity, reduce fatigue resistance, and adversely affect coating adhesion and corrosion performance. In particular, the degradation of surface quality during austenitization can significantly influence subsequent corrosion behavior by promoting localized defects and microstructural discontinuities. Therefore, the application of protective coatings prior to hot stamping is essential to ensure both mechanical reliability and corrosion resistance of HPF steels.

Among various coating systems, Al–Si coatings and Zn-based coatings are the most widely adopted in industrial practice due to their distinct advantages and established processing compatibility. The Al–Si coating, typically composed of Al–10–20 wt% Si, forms stable Fe–Al intermetallic phases such as Al_5Fe_2 and AlFe during high-temperature exposure [4,5]. These intermetallic compounds exhibit low diffusivity and high thermodynamic stability, resulting in the formation of a dense and continuous diffusion layer that effectively suppresses oxidation and acts as a barrier against corrosive

†Corresponding author: khj020911@tukorea.ac.kr
Hye-Jin Kim: Profesor, Ei-Joon Shim: Master degree student, Ho-jun Choi: Master degree student, Yoori Kim: Master degree student

species. In addition, the formation of stable oxide films, including Al_2O_3 and SiO_2, further enhances corrosion resistance by limiting electrolyte penetration and reducing interfacial electrochemical activity.

In contrast, Zn-based coatings, including galvanized (GI) and galvannealed (GA) coatings, provide corrosion protection primarily through a sacrificial anode mechanism [6,7]. In this mechanism, Zn preferentially dissolves in corrosive environments, thereby protecting the underlying steel substrate. While this sacrificial behavior is highly effective in delaying substrate corrosion at the initial stage, it inherently involves continuous consumption of the coating layer. As a result, the long-term durability of Zn coatings is limited, particularly under aggressive environments where rapid dissolution and localized degradation may occur. Furthermore, the relatively low melting point and high diffusivity of Zn during the hot press forming process can lead to the formation of heterogeneous microstructures, which may further influence corrosion behavior.

Previous studies have investigated the corrosion behavior of coated HPF steels using conventional electrochemical techniques such as open circuit potential (OCP), electrochemical impedance spectroscopy (EIS), and potentiodynamic polarization [8-10]. These studies have provided valuable insights into the thermodynamic stability and electrochemical characteristics of coating systems. However, most of the existing works primarily focus on static electrochemical parameters and do not sufficiently capture the dynamic nature of corrosion processes, particularly in systems governed by sacrificial mechanisms. In addition, there has been limited effort to establish a direct correlation between coating microstructure and electrochemical behavior.

In particular, the role of microstructural heterogeneity—such as grain size distribution, phase composition, and interfacial integrity—on corrosion behavior remains insufficiently understood. Advanced characterization techniques such as electron backscatter diffraction (EBSD) provide detailed information on crystallographic orientation, phase distribution, and microstructural uniformity, which are critical factors governing corrosion initiation and propagation. However, the integration of EBSD-derived microstructural features with electrochemical responses, including EIS characteristics and time-dependent corrosion behavior, has not been extensively explored.

Furthermore, while EIS provides information on interfacial resistance and electrochemical processes, it is inherently limited to near-equilibrium conditions. To overcome this limitation, potentiodynamic polarization offers direct insight into corrosion kinetics, including anodic dissolution and cathodic reactions, while galvanostatic testing enables evaluation of coating stability under continuous electrochemical loading conditions. The combination of these techniques allows for a more comprehensive understanding of corrosion mechanisms, particularly in distinguishing between barrier-type protection and sacrificial behavior.

Therefore, the objective of this study is to systematically investigate the correlation between microstructure and corrosion behavior of Al–Si-coated and Zn-coated HPF steels by integrating EBSD-based microstructural analysis with advanced electrochemical techniques. Special emphasis is placed on understanding how microstructural characteristics, including phase distribution and heterogeneity, influence electrochemical responses such as impedance behavior, corrosion kinetics, and time-dependent degradation. By combining EIS, potentiodynamic polarization, and galvanostatic testing with detailed microstructural analysis, this study aims to elucidate the fundamental differences in corrosion mechanisms and provide insights into the design and selection of coating systems for improved long-term durability in automotive applications.

2. Experiment

2.1 Materials and Coating Systems

The base material used in this study was a commercial 22MnB5 press-hardening steel, widely employed in automotive hot-stamping applications. The chemical composition of the steel corresponds to typical boron steel grades designed for martensitic transformation during rapid cooling. Two types of commercially relevant coatings were investigated:

· Al–Si coating: Al–20 wt% Si alloy coating with a coating mass of approximately 40 g/m^2 per side

· Zn coating: Conventional galvannealed coating with Zn, with coating mass of approximately 40 g/m^2 per side

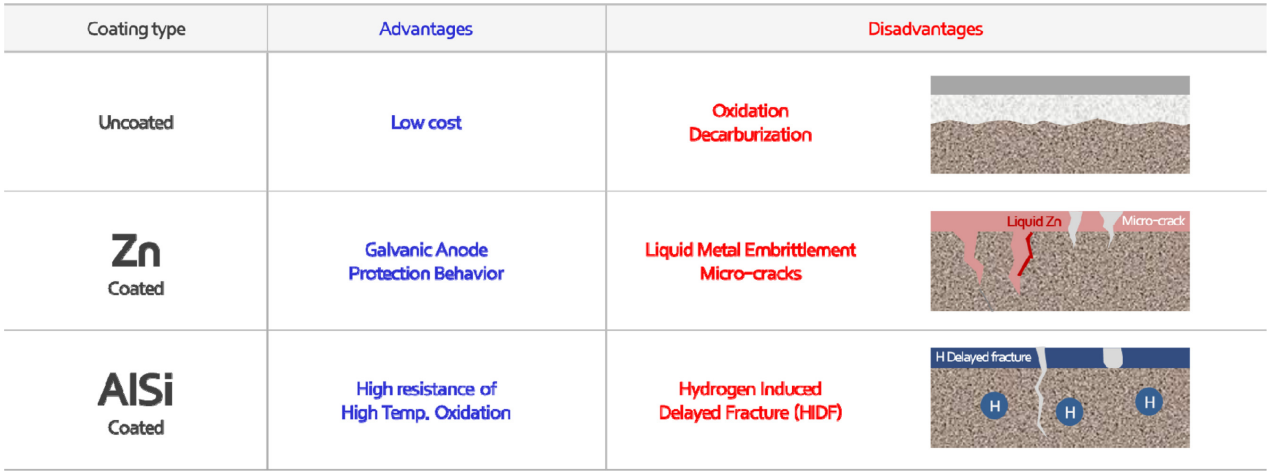

Fig. 1. Comparison of characteristics in uncoated, Zn-coated, and Al–Si-coated hot press forming steels

These coatings were selected due to their widespread industrial use and fundamentally different corrosion protection mechanisms. Fig. 1 schematically compares the corrosion protection mechanisms and associated limitations of uncoated, Zn-coated, and Al–Si-coated hot press forming steels. Uncoated steels exhibit low cost but suffer from severe oxidation and decarburization during high-temperature processing, leading to degraded surface integrity and poor corrosion resistance. The absence of a protective layer allows direct exposure of the substrate to corrosive environments, resulting in rapid degradation.

Zn-coated steels provide corrosion protection primarily through a sacrificial anode mechanism. The preferential dissolution of Zn effectively protects the underlying steel substrate in the initial stages of exposure. However, this mechanism inherently involves continuous consumption of the coating layer. As corrosion progresses, localized dissolution can lead to micro-crack formation and coating discontinuity, which may accelerate degradation and increase susceptibility to localized corrosion and hydrogen-assisted damage.

In contrast, Al–Si-coated steels exhibit superior corrosion resistance due to the formation of a dense Fe–Al intermetallic layer and stable oxide films. These layers act as an effective barrier against the penetration of corrosive species, thereby significantly reducing corrosion kinetics. The coating maintains structural integrity over time, providing stable long-term protection. However, under certain conditions, hydrogen accumulation at the interface may contribute to delayed fracture behavior, although this effect is generally less pronounced compared to the degradation observed in Zn coatings.

Overall, the figure highlights the fundamental difference between sacrificial and barrier-type protection mechanisms, which governs the long-term corrosion performance of coated hot press forming steels.

2.2 Hot Press Forming Process

All coated samples were subjected to identical hot-stamping conditions to ensure a consistent microstructural state of the substrate. The specimens were heated in a furnace to 900 ºC and held for 5 minutes to achieve full austenitization. Subsequently, the samples were rapidly transferred to a die and quenched under pressure, resulting in a fully martensitic microstructure. As shown in Fig. 2, the hot press forming process consists of sequential stages including blank preparation, austenitization, forming/quenching, and trimming, during which significant microstructural evolution occurs not only in the substrate but also within the coating layer. During the heating stage (~900 ºC), the steel substrate undergoes full austenitization, while the coating is exposed to high temperatures for several minutes. At this stage, intensive interdiffusion occurs between the coating and substrate.

For Al–Si coatings, Fe and Al interdiffuse to form Fe–Al intermetallic compounds such as Al_5Fe_2 and AlFe, resulting in the development of a dense diffusion layer. This layer acts as a barrier against further oxidation and element transport. In contrast, Zn coatings experience partial melting or accelerated diffusion due to their

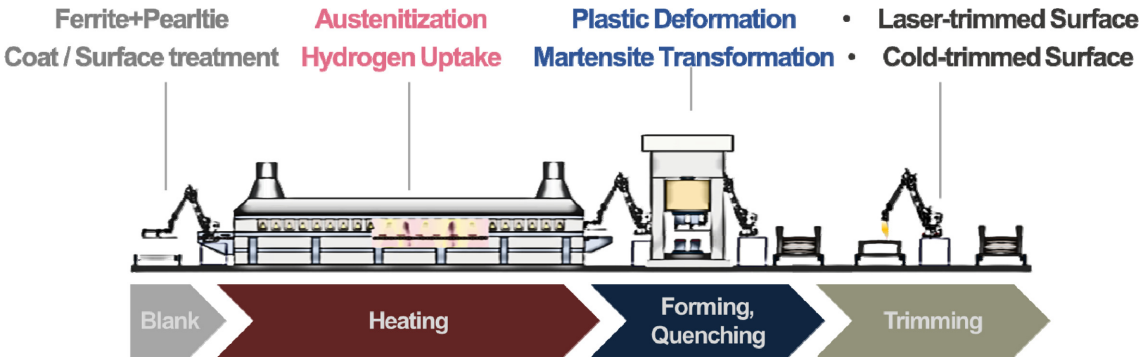

Fig. 2. Schematic illustration of microstructural evolution of coating layers during the hot press forming process, including high-temperature diffusion, phase transformation, and thermo-mechanical damage

relatively low melting point. So, some of parts are evaporated during hot press forming. Fe–Zn intermetallic phases are formed, and surface oxidation (ZnO) may occur simultaneously. This leads to a comparatively less stable and more heterogeneous coating structure.

During the transfer and forming stage, the material undergoes plastic deformation under high temperature conditions. The coating layer is subjected to severe thermo-mechanical stresses due to differences in thermal expansion and mechanical properties between the coating and substrate. As a result, microcracks can form within the coating, particularly in brittle intermetallic layers. These defects may serve as preferential pathways for corrosive species. Simultaneously, rapid die quenching induces martensitic transformation in the substrate. The sudden volume change associated with this transformation can further contribute to stress accumulation at the coating/substrate interface, promoting crack initiation or propagation within the coating layer. After forming, trimming processes such as laser cutting or cold trimming expose fresh surfaces without coating protection, which can act as localized corrosion initiation sites. Therefore, the HPF process not only determines the final microstructure of the substrate but also critically influences the integrity, phase composition, and protective performance of the coating through high-temperature diffusion, phase transformation, and thermo-mechanical damage.

2.3 Microstructural Characterization

The microstructural characteristics of the coatings and substrates were analyzed using a combination of scanning electron microscopy (SEM), electron backscatter diffraction (EBSD), and energy dispersive spectroscopy (EDS). Cross-sectional SEM observations were conducted to examine coating thickness, morphology, and interfacial structure. EBSD analysis was used to identify phase distribution and crystallographic orientation, particularly to confirm the formation of martensitic microstructures in the substrate. EDS mapping was performed to investigate elemental distribution and interdiffusion behavior within the coating layers. Special attention was given to the integrity and continuity of the coating layers, as these factors are critical for corrosion resistance.

2.4 Electrochemical Measurements

All electrochemical tests were performed using a conventional three-electrode cell configuration. The coated specimen served as the working electrode, a saturated calomel electrode (SCE) was used as the reference electrode, and a platinum mesh was employed as the counter electrode. The electrolyte used was naturally aerated 3.5% NaCl solution, prepared using deionized water [11]. Especially, galvanostatic test is performing in electrolyte consisting of 100 g/L $ZnSO_4 \cdot 7H_2O$ and 200 g/L NaCl at 25 ºC The temperature was maintained at 25 ± 1 ºC throughout the experiments [12].

2.4.1 Open Circuit Potential (OCP) and Electrochemical Impedance Spectroscopy (EIS)

The OCP of each specimen was monitored for at least 30 minutes prior to electrochemical measurements to ensure stabilization. This step was essential to establish a steady electrochemical state before subsequent test. EIS

measurements were conducted over a frequency range from 100 kHz to 10 mHz with an AC perturbation amplitude of 10 mV. The obtained impedance spectra were analyzed using an equivalent circuit model.

2.4.3 Potentiodynamic Polarization

Potentiodynamic polarization tests were performed within a potential range of approximately -0.5 ~ 1.0 V_{OCP} with respect to the stabilized OCP at a scan rate of 0.5 mV/s. The corrosion potential (E_{corr}) and corrosion current density (I_{corr}) were determined using Tafel extrapolation. These parameters were used to evaluate the corrosion kinetics and calculate corrosion rates. Special attention was given to the anodic branch behavior, as it directly reflects the dissolution characteristics of the coating materials.

2.4.4 Galvanostatic Testing

Galvanostatic tests were carried out under a constant applied current condition to evaluate the time-dependent electrochemical stability of the coatings. Unlike conventional electrochemical tests, galvanostatic measurements impose a continuous electrochemical load, allowing direct observation of coating degradation behavior over time. The potential response was monitored as a function of time, and fluctuations in potential were analyzed to identify instability, localized corrosion, and coating breakdown phenomena. This method is particularly effective for evaluating sacrificial coatings, where the protective mechanism involves progressive material consumption. Galvanostatic testing was carried out in an electrolyte containing 100 g/L $ZnSO_4 \cdot 7H_2O$ and 200 g/L NaCl at 25 ºC, with a constant applied current density of +11.76 mA/cm^2, to simulate continuous electrochemical loading and assess the degradation behavior of the coatings over time [12].

3. Results and discuSsion

3.1 Microstructure observations

The observed differences in coating morphology can be attributed to the fundamentally different diffusion and phase transformation behaviors during the hot press forming process. In the Zn-coated sample, the coating layer consists of an outer ZnO layer, followed by an Fe–Zn intermetallic region (α-Fe(Zn)), and a diffusion-affected zone near the substrate. The coating appears relatively heterogeneous, with an irregular interface and the presence of defects such as micro-voids and discontinuities. Beneath the coating, a fully transformed α′-martensitic structure is observed in the substrate. In the Zn-coated steel, the formation of Fe–Zn intermetallic phases occur under conditions where Zn has a relatively low melting point and high diffusivity. This leads to rapid phase transformation and the development of a non-uniform microstructure. The presence of ZnO on the surface indicates oxidation during high-temperature exposure. Furthermore, the observed micro-voids and interfacial irregularities suggest that the coating is susceptible to thermo-mechanical instability during forming and quenching. These structural heterogeneities can act as preferential pathways for electrolyte penetration, thereby accelerating localized corrosion.

In contrast, the Al–Si-coated specimen exhibits a well-defined multilayered structure composed of Fe–Al intermetallic phases, including Al_5Fe_2 and AlFe [13]. The coating layer is relatively dense and continuous, with a more uniform interface compared to the Zn-coated sample. The substrate also shows a fully martensitic microstructure, indicating consistent hot press forming conditions. The Al–Si coating forms stable Fe–Al intermetallic compounds through solid-state diffusion at high temperature. These phases are thermodynamically stable and exhibit relatively low diffusivity, resulting in the formation of a dense and continuous coating layer. The compact intermetallic structure effectively suppresses defect formation and provides a robust barrier against corrosive species. Additionally, the uniform interface between the coating and substrate enhances mechanical integrity during deformation, reducing the likelihood of crack initiation.

Therefore, the microstructural characteristics clearly indicate that the Zn coating is more prone to structural degradation due to its heterogeneous and defect-containing nature, whereas the Al–Si coating provides a stable and protective barrier due to its dense intermetallic architecture.

As shown in Fig. 4, EBSD analyses including CI (Confidence index) distribution, inverse pole figure (IPF), and phase maps, reveal distinct microstructural

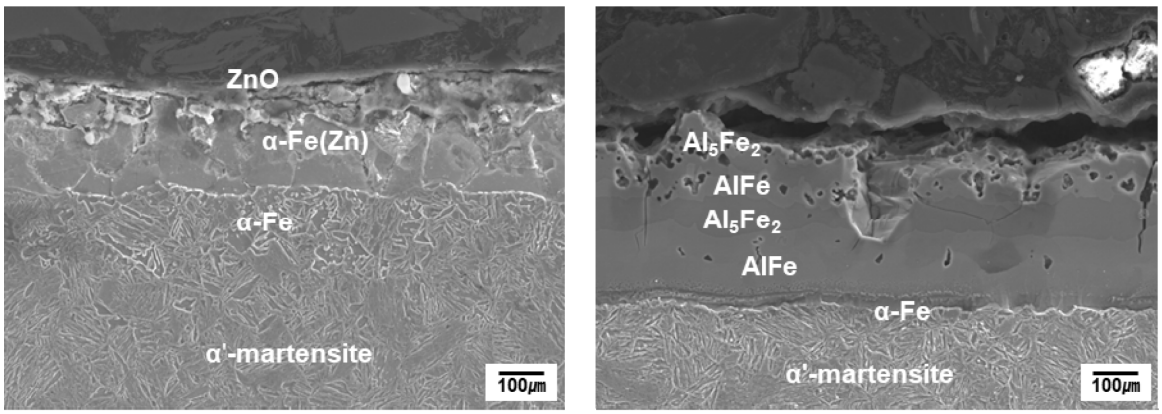

(a) (b)

Fig. 3. Cross-sectional SEM images of (a) Zn-coated and (b) Al–Si-coated hot press forming steels showing distinct coating microstructures and intermetallic phase formation

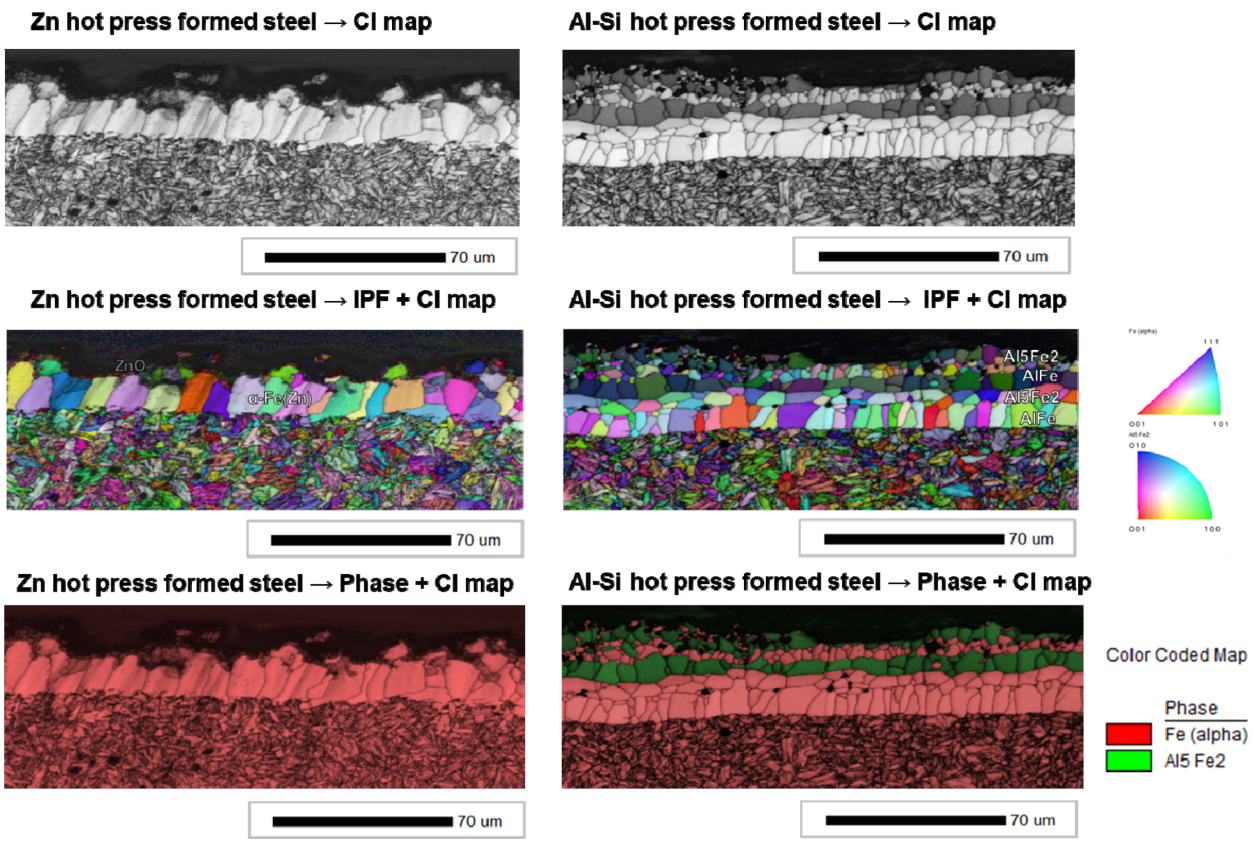

Fig. 4. Cross-sectional microstructural and crystallographic characterization of Zn-coated and Al–Si-coated hot press formed (HPF) steels using EBSD analysis

characteristics between Zn-coated and Al–Si-coated hot press formed steels. In the Zn-coated specimen, the CI map shows a relatively non-uniform distribution, with localized regions of higher intensity near the coating surface and along the coating/substrate interface. The IPF map indicates a coarse and irregular grain structure within the coating layer, with significant orientation heterogeneity. The phase map confirms that the coating region consists primarily of α-Fe(Zn), with no well-defined multilayered structure.

In contrast, the Al–Si-coated specimen exhibits a more uniform surface, with relatively limited penetration into the coating layer. The IPF map reveals a more refined and homogeneous grain structure within the intermetallic coating layer. The phase map clearly identifies a distinct multilayer structure, where the Al_5Fe_2 phase is predominantly formed near the surface, while AlFe is observed closer to the substrate interface. The substrate in both cases consists of fully transformed martensite, indicating consistent thermal processing conditions.

The EBSD results provide strong evidence that the corrosion behavior is governed not only by coating composition but also by microstructural uniformity and phase stability. In the Zn-coated steel, the heterogeneous grain structure and the absence of a well-defined phase hierarchy result in non-uniform electrochemical activity. The heterogeneous surface with large grain boundary of coating suggests that the coating contains preferential pathways for electrolyte penetration. These pathways are likely associated with microstructural discontinuities such as grain boundaries, phase interfaces, and defects formed during high-temperature processing and deformation. Consequently, the Zn coating is more susceptible to localized corrosion and rapid degradation. In contrast, the Al–Si coating exhibits a well-organized multilayered structure composed of stable Fe–Al intermetallic phases. The presence of a continuous Al_5Fe_2 layer near the surface plays a critical role. This phase acts as a dense barrier with low diffusivity, effectively suppressing electrolyte penetration. Furthermore, the relatively uniform grain structure reduces the number of preferential corrosion paths, contributing to enhanced corrosion resistance. The phase distribution also suggests a gradient in mechanical and chemical stability across the coating thickness, which may further improve resistance to thermo-mechanical damage and corrosion propagation.

Therefore, the EBSD results clearly demonstrate that the superior corrosion resistance of the Al–Si coating originates from its dense, multilayered intermetallic structure with fine grain and reduced susceptibility to localized electrolyte penetration, whereas the Zn coating exhibits inherent microstructural heterogeneity with coarsened grain that facilitates corrosion initiation and propagation. Eventually, the heterogeneous microstructure observed in the Zn coating are consistent with its lower impedance and higher corrosion current density, whereas the dense and continuous Al–Si intermetallic layer effectively suppresses electrolyte penetration, resulting in superior electrochemical stability.

Fig. 5 shows EDS elemental mapping based on EBSD analysis that clearly reveals distinct compositional distributions in the coating layers of Zn-coated and Al–Si-coated HPF steels. In the Zn-coated specimen, the Fe map shows a gradual increase toward the substrate, indicating partial interdiffusion between the coating and the base metal. The Zn distribution is relatively diffuse and extends irregularly across the coating layer, suggesting non-uniform diffusion behavior. No distinct compositional layering is observed, and the elemental distribution appears heterogeneous across the thickness. In contrast, the Al–Si-coated specimen exhibits a well-defined multilayered compositional structure. The Fe distribution gradually increases toward the substrate, while Al is highly concentrated within the coating layer, forming a continuous and dense region. The Si distribution is localized within specific regions, consistent with the formation of Fe–Al–Si intermetallic phases. The elemental maps clearly indicate a compositional gradient across the coating thickness, corresponding to the formation of distinct intermetallic layers such as Al_5Fe_2 and AlFe. These results demonstrate that the Al–Si coating forms a structured diffusion layer with clear compositional separation, whereas the Zn coating exhibits a more diffuse and less organized elemental distribution.

The differences in elemental distribution provide critical insight into the formation mechanisms and protective characteristics of the coatings. In the Zn-coated steel, the relatively uniform and diffuse Zn distribution indicates rapid diffusion and possible partial melting during the high-temperature austenitization stage. This leads to the formation of a non-uniform coating structure without a well-defined compositional hierarchy. The lack of a dense and continuous diffusion layer reduces the effectiveness of the coating as a barrier against corrosive species. Furthermore, the heterogeneous distribution can promote localized electrochemical activity, thereby accelerating corrosion initiation.

In contrast, the Al–Si coating exhibits a highly organized diffusion structure, where Al is concentrated in a continuous layer that acts as a primary barrier. The

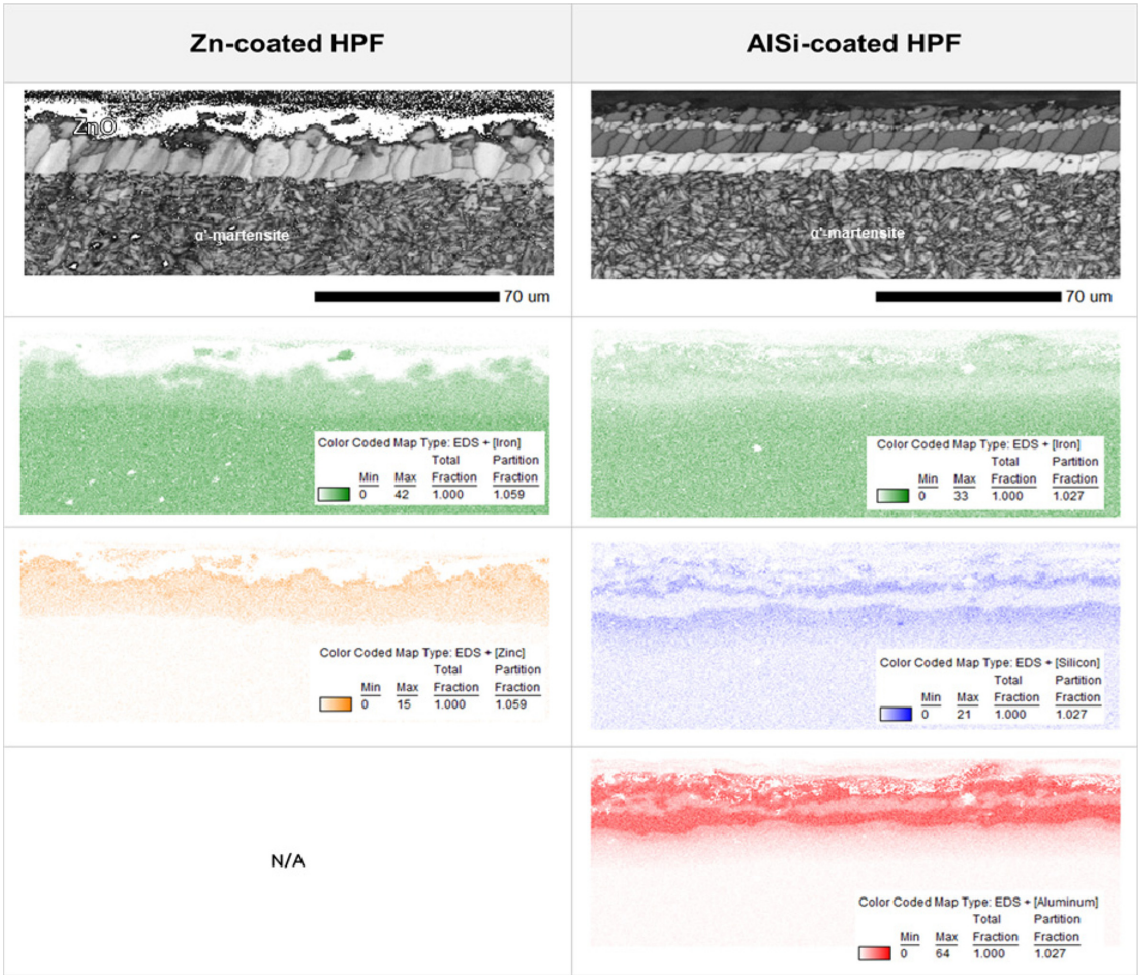

Fig. 5. EDS elemental maps of Zn-coated and Al–Si-coated hot press formed steels showing distinct compositional distributions and diffusion layer formation

presence of Si further stabilizes the intermetallic phases and contributes to the formation of a compact microstructure. The gradual Fe concentration profile indicates controlled interdiffusion, resulting in the formation of stable Fe–Al intermetallic compounds. This structured compositional gradient significantly enhances corrosion resistance by limiting electrolyte penetration and suppressing localized corrosion. The dense Al-rich layer acts as an effective diffusion barrier, while the multilayered structure improves mechanical stability during deformation. Therefore, the EDS results confirm that the superior corrosion resistance of the Al–Si coating originates from its well-defined diffusion layer and compositional stability, whereas the Zn coating lacks a coherent barrier structure due to its diffuse elemental distribution.

3.2 Electrochemical test results

The evolution of OCP as a function of immersion time for Zn-coated and Al–Si-coated HPF steels is shown in Fig. 6. The Al–Si-coated specimen exhibits a relatively noble potential, initially around –0.50 V_{SCE} (vs. SCE), followed by a gradual decrease toward approximately –0.62 V_{SCE} with increasing immersion time. The potential change is smooth and continuous, indicating a stable electrochemical state without significant fluctuations. In contrast, the Zn-coated specimen shows a much more negative potential, approximately –0.85 V_{SCE}, which remains relatively stable over time with only minor variation. The potential difference between the two coatings is approximately 0.3 – 0.35 V_{SCE} throughout the test duration. The significant difference in OCP behavior reflects the fundamentally different corrosion protection

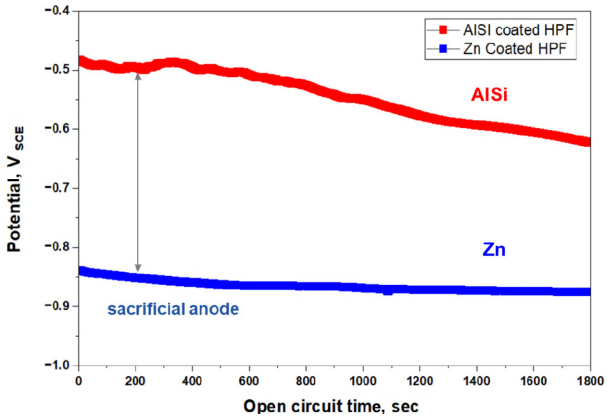

Fig. 6. Open circuit potential (OCP) evolution of Zn-coated and Al–Si-coated hot press formed steels in 3.5 wt% NaCl solution

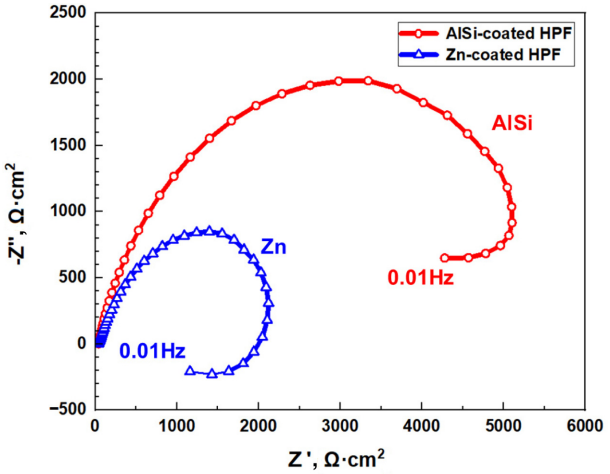

Fig. 7. Nyquist plots of Zn-coated and Al–Si-coated hot press formed steels in 3.5 wt% NaCl solution

mechanisms of the two coatings.

The more negative potential of the Zn-coated specimen is characteristic of its sacrificial anode behavior. Zn preferentially undergoes anodic dissolution, thereby protecting the underlying steel substrate. The relatively stable but low potential suggests continuous electrochemical activity, indicating that the coating is actively corroding throughout the exposure period. In contrast, the Al–Si-coated specimen exhibits a more noble potential, which is indicative of a barrier-type protection mechanism. The gradual decrease in potential over time can be attributed to surface stabilization processes, such as the formation and evolution of passive oxide layers. The absence of abrupt potential fluctuations suggests that the coating maintains its structural integrity and effectively suppresses localized corrosion.

Importantly, the large potential gap between the two coatings (~300 mV) confirms that the Zn coating is electrochemically more active, whereas the Al–Si coating is significantly more stable. This difference directly correlates with the microstructural observations, where the dense and continuous Al–Si intermetallic layer limits electrolyte penetration, while the heterogeneous Zn coating facilitates electrochemical reactions. he more negative OCP of the Zn coating is consistent with its heterogeneous microstructure observed in the EBSD and EDS analyses, whereas the relatively noble and stable potential of the Al–Si coating reflects the effectiveness of its dense intermetallic diffusion layer as a corrosion barrier

The Nyquist plots of Zn-coated and Al–Si-coated HPF steels obtained in 3.5 wt% NaCl solution are shown in Fig. 7.

The Al–Si-coated specimen exhibits a significantly larger semicircular arc compared to the Zn-coated specimen, indicating a much higher impedance response. The diameter of the semicircle, which corresponds to the charge transfer resistance (R_{ct}), is markedly higher for the Al–Si coating, reaching values above 4000 Ω·cm^2. In contrast, the Zn-coated specimen shows a considerably smaller semicircle with a diameter of approximately 1500 – 2000 Ω·cm^2, suggesting lower resistance to charge transfer. Both samples exhibit a single depressed semicircle, indicating non-ideal capacitive behavior associated with surface heterogeneity and the presence of constant phase elements (CPE).

The significantly higher impedance of the Al–Si-coated specimen indicates superior corrosion resistance, primarily due to its barrier-type protection mechanism. The large semicircle reflects a high charge transfer resistance, suggesting that electrochemical reactions at the interface are strongly suppressed. This behavior is consistent with the dense and continuous Fe–Al intermetallic layer observed in SEM and EDS analyses, which effectively limits electrolyte penetration and reduces active corrosion sites. In contrast, the Zn-coated specimen exhibits much lower impedance, indicating active electrochemical processes at the coating surface. The smaller semicircle suggests a lower charge transfer resistance, which can be attributed to the sacrificial dissolution of Zn. The heterogeneous microstructure and

localized defects identified in EBSD and SEM observations provide preferential pathways for electrolyte ingress, facilitating charge transfer reactions. Furthermore, the depressed nature of the semicircles suggests surface inhomogeneity, which is more pronounced in the Zn-coated sample. This supports the presence of localized corrosion activity and non-uniform degradation behavior.

At low frequencies (0.01 Hz), the Al–Si-coated specimen maintains a high impedance value, indicating strong resistance to long-term corrosion processes. This suggests that the coating effectively suppresses diffusion-controlled reactions and maintains its protective integrity over extended exposure. In contrast, the Zn-coated specimen shows significantly lower impedance at low frequencies, indicating reduced resistance to corrosion propagation. This behavior reflects the continuous consumption of the Zn coating and the limited long-term stability of the sacrificial protection mechanism. The higher impedance of the Al–Si coating is consistent with its dense and continuous intermetallic structure observed in SEM and EDS analyses, whereas the lower impedance of the Zn coating correlates with its heterogeneous microstructure revealed by EBSD results.

The EIS data were fitted using ZView4, and different equivalent electrical circuits were selected for the two coating systems because the impedance responses were clearly governed by different electrochemical processes in Fig. 8. As shown in Fig. 8a**,** the Al–Si-coated HPF steel was adequately described by a relatively simple circuit consisting of the solution resistance R_s, one constant phase element (QPE_1), and one resistance term R_1. This type of circuit is generally associated with an electrochemical interface dominated by a stable interfacial charge-transfer process. In other words, the impedance response of the Al–Si-coated steel can be interpreted as arising mainly from one dominant time constant, which is consistent with a comparatively uniform and compact surface layer. By contrast, the Zn-coated HPF steel required a more complex circuit composed of R_s, CPE_1, R_1, L_2, and R_2 in. The need for an inductive element in the Zn-coated sample is particularly meaningful. In electrochemical systems, an inductive loop at low frequency is often associated with adsorption/desorption of intermediate species, local dissolution events, or unstable surface reactions during active corrosion [14]. Therefore, the Zn-coated HPF steel could not be represented solely by a simple electrochemical interface model. Instead, its response was better interpreted using an adsorption-involved model, indicating that the corrosion of the Zn-coated layer proceeded through a more dynamic and unstable surface process than that of the Al–Si-coated steel.

The fitting quality was very good for both coating systems. In the Nyquist and Bode plots shown in Fig. 8b and c, the fitted curves closely overlapped the experimental data over almost the entire frequency range. This result indicates that the selected equivalent circuits appropriately describe the electrochemical behavior of each coating and that the extracted fitting parameters are physically meaningful. The fitting reliability is also supported by the low error percentages listed in Tables 1 and 2. For the Al–Si-coated HPF steel referred to Fig. 8b and Table 1, the fitted parameters were R_s=44.09 Ω with an error of 0.68%, $QPE_1 - Q = 7.564 \times 10^{-6}$ $F \cdot s^{n-1}$with an error of 3.18%, QPE_1-n=0.79 with an error of 0.30%, and R_1 = 5350 Ω with an error of 0.95%. These values indicate a highly resistive electrochemical interface. In particular, the very large R_1 value suggests that the Al–Si-coated HPF steel possesses strong resistance against interfacial charge transfer, which directly corresponds to low corrosion kinetics. The n value of 0.79 also indicates that the interfacial response is close to capacitive behavior, although not ideally so, implying that the surface is relatively homogeneous but still contains some degree of roughness or structural heterogeneity, as expected in real hot-stamped intermetallic coatings. For the Zn-coated HPF steel in Table 2, the fitted parameters were R_s=41.96 Ω with an error of 0.83%, $CPE_1 - Q = 2.793 \times 10^{-4}$ $F \cdot s^{n-1}$with an error of 2.12%, CPE_1-n=0.70 with an error of 0.70%, R_1=1463 Ω with an error of 3.15%, L_2 = 5997 H with an error of 9.89%, and R_2 = 1192 Ω with an error of 5.28%. Several points are noteworthy here. First, the resistance terms in the Zn-coated HPF steel are much smaller than the R_1 value of the Al–Si-coated steel. Even if R_1 and R_2 in the Zn-coated steel are considered together, the overall interfacial resistance remains significantly lower than that of the Al–Si-coated steel. Second, the P value of 0.70 is lower than the n value obtained for the Al–Si-coated steel, suggesting a more non-ideal interfacial behavior, which is consistent with a rougher,

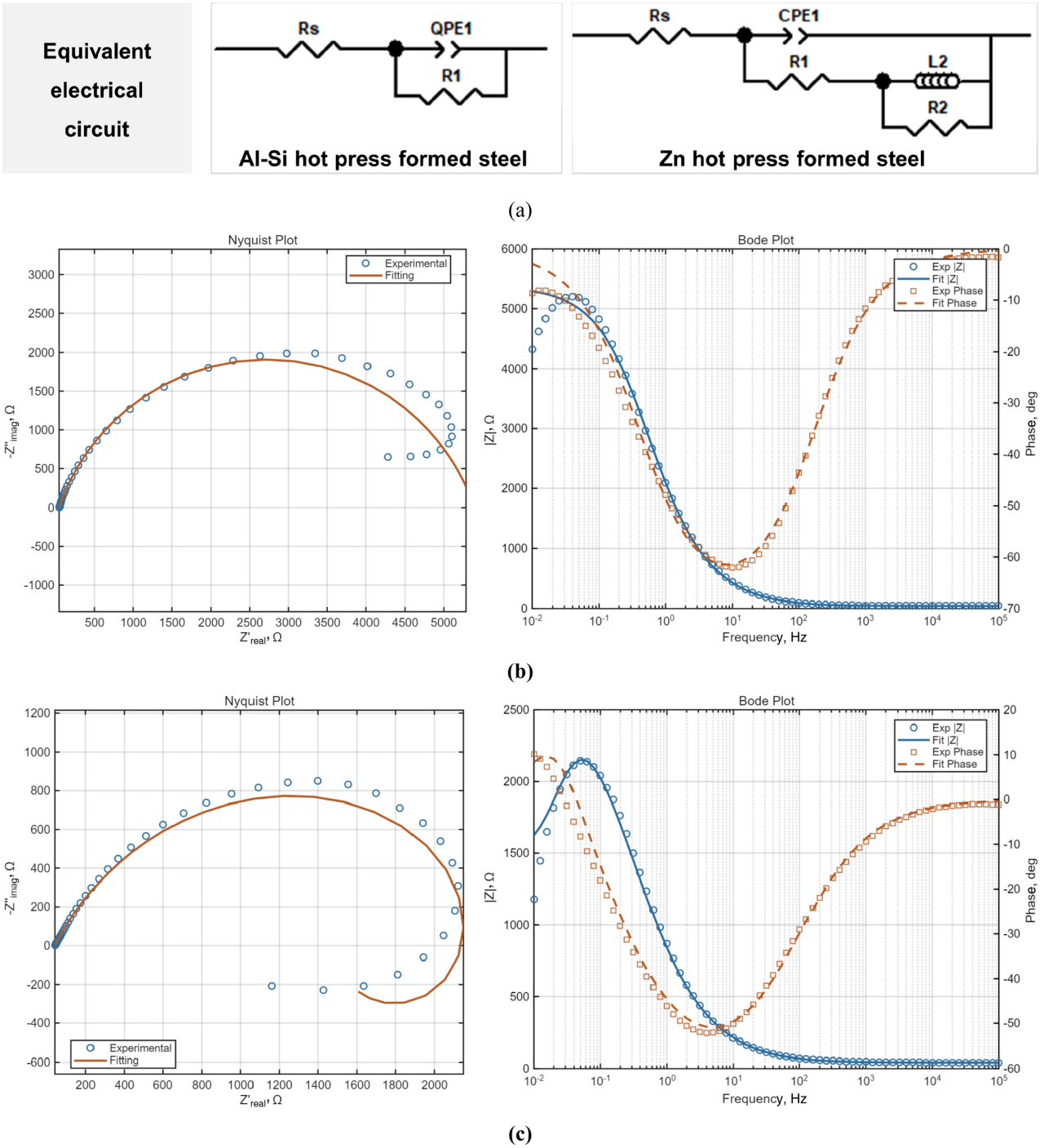

Fig. 8. EIS fitting graph; (a) Equivalent electrical circuits used for EIS fitting of Al–Si- and Zn-coated HPF steels; (b) Nyquist and Bode plots of Al–Si-coated HPF steel with experimental and fitted data; (c) Nyquist and Bode plots of Zn-coated HPF steel with experimental and fitted data

less uniform, and electrochemically less stable surface. Third, the presence of the inductive element L_2 strongly supports the interpretation that the Zn-coated steel undergoes adsorption-related intermediate reactions during corrosion, which are absent, or at least not dominant, in the Al–Si-coated system.

The Nyquist plots provide an especially clear comparison between the two coatings. The Al–Si-coated HPF steel shows a much larger capacitive arc than the Zn-coated sample, demonstrating greater polarization resistance

and more effective suppression of electrochemical reactions. The Bode magnitude plot also confirms that the impedance modulus of the Al–Si-coated sample remains higher across a broad frequency range, which is a typical feature of a more protective surface film or barrier layer. In contrast, the Zn-coated HPF steel displays a smaller arc radius and a more complex low-frequency response, which suggests greater electrochemical instability and participation of additional interfacial processes. The physical meaning of these EIS results becomes much clearer when they are correlated with the EBSD and phase mapping results. In the Al–Si-coated HPF steel, the phase maps indicate the presence of Fe–Al intermetallic compounds such as Al_5Fe_2 and AlFe above the martensitic substrate. The coating region appears relatively continuous and stratified, and chloride distribution is less suggestive of deeply localized penetration. In other words, the Al–Si coating forms a comparatively dense intermetallic barrier that separates the external chloride-containing electrolyte from the steel substrate. Because the interface is relatively compact and continuous, the electrochemical response is governed mainly by a single interfacial process, which explains why the simpler R_s-QPE_1-R_1 model successfully reproduces the EIS spectra.

On the other hand, the Zn-coated HPF steel shows a coating structure containing α-Fe(Zn), ZnO, and Zn-related transformed layers after hot press forming. Compared with the Al–Si-coated steel, the Zn-coated specimen exhibits greater microstructural heterogeneity, and the chloride map suggests more localized chloride accumulation near the outer and intermediate coating region. This heterogeneous microstructure provides multiple possible reaction sites during immersion. Local dissolution of Zn-rich areas, formation and breakdown of corrosion products, and adsorption of intermediate species can all occur simultaneously or sequentially. This explains why the Zn-coated HPF steel does not show a simple one-time-constant behavior, but rather requires a more complicated circuit including an inductive element. Thus, the EIS response is directly linked to the non-uniformity and chemical reactivity of the Zn-derived coating layer.

Overall, the corrosion mechanism can be described as follows. The Al–Si-coated HPF steel develops a dense Fe–Al intermetallic coating layer after austenitization and die quenching. This layer acts as a physical and electrochemical barrier, limiting chloride ingress and suppressing interfacial charge transfer. As a result, the Al–Si-coated sample exhibits a large impedance arc and high fitted resistance behavior. In contrast, the Zn-coated HPF steel relies on sacrificial protection. Although this mechanism may provide initial anodic protection, the Zn-derived coating layer is prone to adsorption-related transient processes during corrosion. Consequently, the Zn-coated sample exhibits lower impedance, smaller resistance values and stronger non-ideal interfacial behavior. From the viewpoint of structure-property correlation, the EBSD and phase maps explain why the Al–Si-coated steel behaves as an interface-controlled passive/barrier system, whereas the Zn-coated steel behaves as an adsorption-involved active corrosion system. The compact Al_5Fe_2/AlFe intermetallic layer in the Al–Si-coated steel provides a more continuous barrier and thus supports a simpler, high-resistance electrochemical response. In contrast, the Zn-derived multiphase layer containing α-Fe(Zn), ZnO, and transformed Zn-rich phases promotes local electrochemical heterogeneity and therefore leads to a more complex impedance response with an inductive contribution. Accordingly, the EIS fitting results not only confirm that the Al–Si-coated HPF steel has better corrosion resistance than the Zn-coated HPF steel, but also provide mechanistic evidence for why this difference arises. The superior corrosion resistance of the Al–Si-coated HPF steel originates from the formation of a dense and stable intermetallic barrier layer, while the inferior corrosion resistance of the Zn-coated HPF steel is associated with its sacrificial dissolution behavior, adsorption-related interfacial instability, and more heterogeneous coating microstructure.

The potentiodynamic polarization curves of Zn-coated and Al–Si-coated HPF steels in 3.5 wt% NaCl solution are shown in Fig. 9. The Al–Si-coated specimen exhibits a significantly more noble corrosion potential than the

Table 1. Fitted electrochemical parameters of Al–Si-coated HPF steel obtained from Nyquist and Bode plot analysis using the equivalent circuit model. (Values in parentheses indicate fitting error, %)

Parameter	R_s (Ω)	QPE_1-Q ($F \cdot s^{n-1}$)	QPE_1-n (-)	R_1 (Ω)
Al-Si coated HPF	44.09 (0.68)	7.56E-6 (3.18)	0.79 (0.39)	5350 (0.95)

Table 2. Fitted electrochemical parameters of Zn-coated HPF steel obtained from Nyquist and Bode plot analysis using the equivalent circuit model. (Values in parentheses indicate fitting error, %)

Parameter	R_s (Ω)	CPE_1-Q ($F \cdot s^{n-1}$)	CPE_1-n (-)	R_1 (Ω)	L_2 (H)	R_2 (Ω)
Zn coated HPF	41.96 (0.83)	2.79E-4 (2.12)	0.70 (0.69)	1463 (3.15)	5997 (9.89)	1122 (5.28)

Zn-coated specimen. The corrosion potential difference between the two coatings is approximately 0.2–0.3 V_{SCE}, indicating a clear electrochemical distinction between the barrier-type Al–Si coating and the sacrificial Zn coating. In the anodic branch, the Zn-coated specimen shows a rapid increase in anodic current density immediately after polarization, indicating active dissolution of the Zn layer. By contrast, the Al–Si-coated specimen maintains a relatively lower anodic current response over a wider potential range, suggesting a greater resistance to anodic dissolution. In the cathodic region, the Zn-coated specimen also shows higher electrochemical activity, whereas the Al–Si-coated specimen exhibits a relatively suppressed current response. Overall, the polarization behavior indicates that the Al–Si-coated HPF steel has lower corrosion kinetics and higher electrochemical stability than the Zn-coated HPF steel.

The polarization results clearly demonstrate the fundamentally different corrosion mechanisms of the two coatings. The Zn-coated HPF steel exhibits a much more negative corrosion potential, which is characteristic of sacrificial anodic protection. This means that Zn is electrochemically more active than the underlying steel and preferentially dissolves when exposed to the chloride-containing electrolyte. The steep anodic branch confirms that once polarization begins, the Zn coating undergoes rapid dissolution. Although this sacrificial behavior can temporarily protect the substrate, it also means that the coating is continuously consumed, which limits long-term durability.

In contrast, the Al–Si-coated HPF steel shows a more noble corrosion potential and a significantly reduced anodic current response. This indicates that the Al–Si coating is not acting as a sacrificial layer, but rather as a barrier-type protective layer that suppresses interfacial electrochemical reactions. The relatively stable anodic behavior suggests that the dense Fe–Al intermetallic layer and the associated oxide film reduce metal dissolution and retard corrosion propagation.

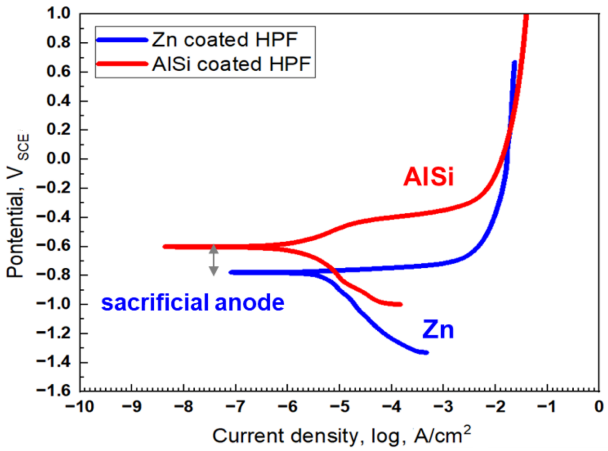

Fig. 9. Potentiodynamic polarization curves of Zn-coated and Al–Si-coated hot press formed steels in 3.5 wt% NaCl solution

The Tafel extrapolation of the polarization curves provides quantitative support for the above interpretation in Table 3. From the exact fitting values, the polarization curves clearly indicate that the Al–Si-coated specimen has a lower corrosion current density (i_{corr}) and a more noble corrosion potential (E_{corr}) than the Zn-coated specimen. A lower I_{corr} value for the Al–Si-coated specimen implies a lower corrosion rate, confirming its superior corrosion resistance. In contrast, the higher I_{corr} of the Zn-coated specimen reflects accelerated corrosion kinetics associated with sacrificial Zn dissolution.

Therefore, the potentiodynamic polarization curves confirm that the Zn coating provides protection through active sacrificial dissolution, whereas the Al–Si coating suppresses corrosion by forming a stable barrier against anodic metal dissolution. The lower anodic current density of the Al–Si-coated specimen indicates improved resistance to coating degradation, which is attributed to the dense Fe–Al intermetallic layer formed during hot press forming. In contrast, the Zn-coated specimen exhibits rapid anodic dissolution, indicating that its

Table 3. Calculated parameters (corrosion potential and corrosion rate) from potentiodynamic using Tafel Fit

Parameter	E_{corr} (V)	i_{corr} (μA/cm^2)	Corrosion rate (mpy)	ba (V/dec)	bc (V/dec)
Al-Si coated HPF	-0.602	1.37	0.624	0.14	0.22
Zn coated HPF	-0.896	2.75	1.253	0.05	0.27

corrosion protection is achieved at the expense of continuous coating consumption. The more negative corrosion potential of the Zn-coated specimen is also consistent with its OCP behavior, which remained at a significantly lower potential throughout immersion, confirming its sacrificial anode character. The polarization results are in good agreement with the EIS analysis. The higher barrier resistance and charge transfer resistance of the Al–Si-coated specimen is reflected in its lower corrosion current density and more noble corrosion potential, whereas the lower impedance of the Zn-coated specimen corresponds to its active anodic dissolution and higher corrosion kinetics.

The galvanostatic response of Zn-coated and Al–Si-coated HPF steels under a constant applied current density of 11.76 mA/cm^2 is shown in Fig. 10. The Zn-coated specimen initially exhibits a highly negative potential (~ –0.65 V_{SCE}), followed by a rapid increase toward more noble values within the first 1000 s. After this transient stage, the potential gradually stabilizes around –0.25$_{SCE}$ to –0.30 V $_{SCE}$ with noticeable fluctuations. In contrast, the Al–Si-coated specimen shows a relatively stable potential from the initial stage (~ –0.40 V_{SCE}), with only a slight increase over time and minimal fluctuation throughout the test duration. A crossover point is observed at approximately 1000–1500 s, where the potential of the Zn-coated specimen becomes comparable to or slightly higher than that of the Al–Si-coated specimen.

The galvanostatic results clearly reveal the fundamental difference in time-dependent corrosion behavior between the two coating systems. The Zn-coated specimen shows a typical sacrificial anode behavior. The initial highly negative potential corresponds to active Zn dissolution under applied current. As the Zn layer is progressively consumed, the coating loses its sacrificial capability, leading to a gradual shift toward more noble potentials. The observed potential increase and fluctuations indicate coating degradation, localized breakdown, and exposure of the underlying substrate. This behavior confirms that

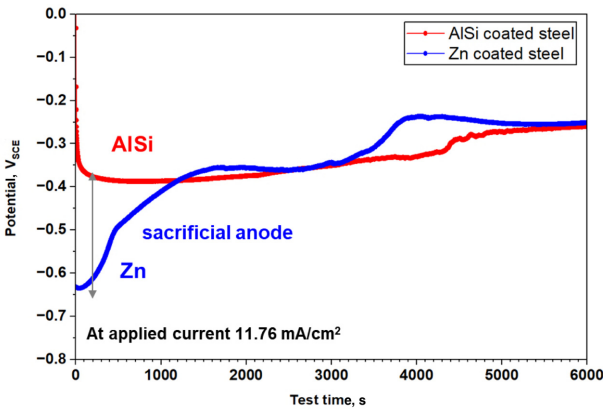

Fig. 10. Galvanostatic response of Zn-coated and Al–Si-coated hot press formed steels at a constant current density of 11.76 mA/cm^2 in solution of in 100 g/L $ZnSO_4$*7H_2O + 200 g/L NaCl

Zn coatings provide only transient protection, as their corrosion resistance is directly dependent on the remaining coating thickness. In previous studies, it has been reported that the addition of alloying elements such as Zn in Al–Si coatings significantly influence corrosion potential and corrosion rate through micro-galvanic interactions within the coating layer [15]. Previous studies have shown that oxide layers formed during hot stamping of Zn-coated steels, such as ZnO and $ZnAl_2O_4$, play a critical role in determining corrosion resistance by affecting diffusion and barrier properties [16]. Therefore, considering that Zn addition provides both sacrificial protection and barrier effects, it is expected that such mechanisms can be effectively extended to other coating systems for enhanced corrosion resistance.

In contrast, the Al–Si-coated specimen maintains a relatively stable potential throughout the test, indicating that the coating does not rely on sacrificial dissolution. Instead, the Al–Si coating provides protection through a barrier-type mechanism, where the dense Fe–Al intermetallic layer suppresses electrochemical reactions and limits electrolyte penetration. The absence of significant potential fluctuations further suggests that the coating remains structurally intact under continuous

electrochemical loading, demonstrating superior long-term stability.

The galvanostatic results provide direct evidence that the superior corrosion resistance of the Al–Si coating is not only associated with its higher impedance and lower corrosion current density, but also with its ability to maintain structural and electrochemical stability under continuous electrochemical loading, unlike the Zn coating which undergoes progressive degradation due to sacrificial dissolution. Although the Zn coating exhibits sacrificial protection at the initial stage, its protective effect diminishes over time due to continuous consumption, whereas the Al–Si coating maintains stable protection without significant degradation."

4. Conclusions

The corrosion behavior and microstructural characteristics of Zn-coated and Al–Si-coated hot press forming (HPF) steels were systematically investigated using combined microstructural and electrochemical analyses. The following conclusions can be drawn:

The Al–Si coated HPF formed a dense and continuous Fe–Al intermetallic diffusion layer (Al_5Fe_2 and AlFe), whereas the Zn coated HPF exhibited a heterogeneous microstructure with Fe–Zn phases and surface oxides, accompanied by defects and discontinuities. EBSD and EDS analyses revealed that the Al–Si coating effectively suppressed corrosion due to its well-defined multilayered structure and fine grain, while the Zn coated HPF showed heterogeneous surface associated with its non-uniform microstructure and coarsened grain.

EIS analysis revealed a clear difference in electrochemical behavior between the two coatings. The Al–Si-coated HPF showed a relatively simple and stable impedance response characterized by a single dominant time constant, indicating that the corrosion process is mainly governed by a stable charge transfer at a compact electrochemical interface. In contrast, the Zn coated HPF exhibited a more complex impedance behavior with multiple time constants and the presence of adsorption-related processes, suggesting a heterogeneous and dynamically evolving interface during corrosion.

Potentiodynamic polarization results showed that the Zn coated HPF undergoes active anodic dissolution due to its sacrificial nature, whereas the Al–Si coated HPF maintains a stable electrochemical response by inhibiting anodic reactions. Galvanostatic testing revealed that the Zn-coated HPF provides only transient protection due to continuous consumption, while the Al–Si coated HPF maintains stable protection under sustained electrochemical loading.

Overall, the superior corrosion resistance of the Al–Si coated HPF originates from its dense intermetallic barrier structure and long-term electrochemical stability, whereas the Zn coating is governed by a sacrificial mechanism that limits its durability.

These findings demonstrate that Al–Si coated HPF provide fundamentally superior long-term corrosion protection compared to Zn coated HPF due to their barrier-type mechanism and structural stability under both static and dynamic electrochemical conditions

Acknowledgments

This work was supported by Korea institute for Advancement of Technology (KIAT) grant funded by the Korea Government(MOTIE) (RS-2024-00410332, HRD Program for Industrial Innovation).

References

1. H. Karbasian, A. E. Tekkaya, A Review on Hot Stamping, *Journal of Materials Processing Technology*, **210**, 2103 (2010). Doi: https://doi.org/10.1016/j.jmatprotec.2010.07.019
2. C. Ying, Z. H. Meng, L. Ying, X.-D. Li, N. Ma, P. Hu, Influence of Hot Press Forming Techniques on Properties of Vehicle High Strength Steels, *Journal of Iron and Steel Research International*, **18**, 59 (2011). Doi: https://doi.org/10.1016/S1006-706X(11)60066-6
3. D. W. Fan, H. S. Kim, J.-K. Oh, K.-G. Chin, B. C. De Cooman, Coating Degradation in Hot Press Forming, *ISIJ International*, **50**, 561 (2010)., Doi: https://doi.org/10.2355/isijinternational.50.561
4. W. Yang, J, Lee, C. Kim, S. Ahn, C. Homero, Effects of Adding Mg to AlSi Coating for Hot Stamping Steel, *Corrosion Science and Technology*, **20**, 196 (2021). Doi: https://doi.org/10.14773/cst.2021.20.4.196
5. S. Wu, Z. Zhou, N. Bruce, A. Bardelcik, C. Chiriac, C.

Shi, A simulation of Al-Si coating growth under various hot stamping austenitization parameters: An artificial neural network model, *Materialstoday Communications*, **38**, 108492 (2024). Doi: https://doi.org/10.1016/j.mtcomm.2024.108492

6. H. Nam, M. Seo, C. Park, Effect of Cold-Sprayed Zinc Coating and Heat Treatment on the Microstructure and Corrosion Behavior of 30MnB5 Hot-Stamped Steel, *Materials*, **18**, 5032 (2025). Doi: https://doi.org/10.3390/ma18215032
7. L. Chen, W. Chen, M. Cao, X. Li, Performance Comparison of Zn-Based and Al-Si Based Coating on Boron Steel in Hot Stamping, *Materials*, **14**, 7043 (2021). Doi: https://doi.org/10.3390/ma14227043
8. S. Hayashida, T. Mitsunobu, H. Takebayashi, Structure of Surface Oxide Formed on Zinc-Coated Steel Sheet During Hot Stamping, *Corrosion Science and Technology*,**23**, 221 (2024). Doi: https://doi.org/10.14773/CST.2024.23.3.221
9. L. Dosdat, J. Petitjean, T. Vietoris, O. Clauzeau, Corrosion Resistance of Different Metallic Coatings on Press-Hardened Steels for Automotive, *Steel research international*, **82**, 726 (2011). Doi: https://doi.org/10.1002/srin.201000291
10. J.-S. Park, H. J. Lee, S. J. Kim, Electrochemical Corrosion and Hydrogen Diffusion Behaviors of Zn and Al Coated Hot-Press Forming Steel Sheets in Chloride Containing Environments, *Korean Journal of Materials Research*, **28**, 286 (2018). Doi: https://doi.org/10.3740/MRSK.2018.28.5.286
11. ASTM G5-14, Standard Reference Test Method for Making Potentiostatic and Potentiodynamic Polarization Measurements. ASTM International: West Conshohocken, PA, USA, 2014. Available online: https://www.astm.org/g0005-94r11e01.html (accessed on 22 October 2025).
12. T. Kurz1, H. Schwinghammer, G. Luckeneder, T. Manzenreiter, A. Sommer, Zinc Coated Press-hardening Steel Challenges and Solution, *Proc. SAE 2015 World Congress & Exhibition*, Detroit, Michigan, United States, April 21 (2015). Doi: https://doi.org/10.4271/2015-01-0565
13. M. Windmann, A. Röttger, W. Theisen, Formation of intermetallic phases in Al-coated hot-stamped 22MnB5 sheets in terms of coating thickness and Si content, *Surface & Coatings Technology*, **246**, 17 (2014). Doi: http://dx.doi.org/10.1016/j.surfcoat.2014.02.056
14. Héctor Herrera Hernández, Adriana M. Ruiz Reynoso, Juan C. Trinidad González, Carlos O. González Morán, José G. Miranda Hernández, Araceli Mandujano Ruiz, Jorge Morales Hernández and Ricardo Orozco Cruz, Electrochemical Impedance Spectroscopy (EIS): A Review Study of Basic Aspects of the Corrosion Mechanism Applied to Steels, *Electrochemical Impedance Spectroscopy*, p. ?? (2020). Doi: http://dx.doi.org/10.5772/intechopen.94470
15. S. Lee, J. Jin, E. Wang, Y., Choi, H. Jang, Corrosion Behavior of Al-Si Coatings with Different Mg and Zn Contents, *Corrosion Science and Technolog*, **24**, 478 (2025). Doi: https://doi.org/10.14773/CST.2025.24.6.478
16. S. Hayashida, T. Mitsunobu, H. Takebayashi, Structure of Surface Oxide Formed on Zinc-Coated Steel Sheet During Hot Stamping, *Corrosion Science and Technology*, **23**, 221 (2024). Doi: https://doi.org/10.14773/cst.2024.23.3.221